JACS
JOURNAL OF THE AMERICAN CHEMICAL SOCIETY
Article
pubs.acs.org/JACS

Chemical Intercalation of Zerovalent Metals into 2D Layered Bi_2Se_3 Nanoribbons

Kristie J. Koski,[†] Colin D. Wessells,[†] Bryan W. Reed,[‡] Judy J. Cha,[†] Desheng Kong,[†] and Yi Cui*[,†,§]

[†]Department of Materials Science and Engineering, Stanford University, Stanford, California 94305, United States

[‡]Physical and Life Sciences Directorate, Lawrence Livermore National Laboratory, 7000 East Avenue, Livermore, California 94550, United States

[§]SLAC National Accelerator Laboratory, Stanford Institute for Materials and Energy Sciences, 2575 Sand Hill Road, Menlo Park, California 94025, United States

Supporting Information

ABSTRACT: We have developed a chemical method to intercalate a variety of zerovalent metal atoms into two-dimensional (2D) layered Bi_2Se_3 chalcogenide nanoribbons. We use a chemical reaction, such as a disproportionation redox reaction, to generate dilute zerovalent metal atoms in a refluxing solution, which intercalate into the layered Bi_2Se_3 structure. The zerovalent nature of the intercalant allows superstoichiometric intercalation of metal atoms such as Ag, Au, Co, Cu, Fe, In, Ni, and Sn. We foresee the impact of this methodology in establishing novel fundamental physical behaviors and in possible energy applications.

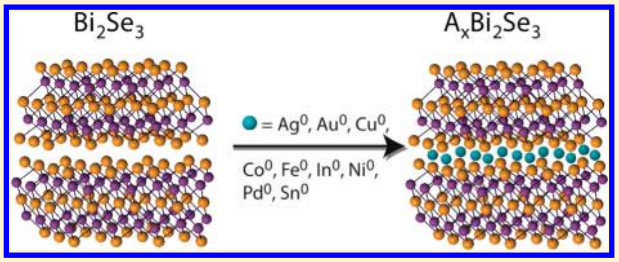

1. INTRODUCTION

Intercalation is the insertion of a guest species into a host lattice. Intercalation into layered materials is essential to battery electrodes, electrochromics, detergents, and solid lubricants and is important in exotic fundamental two-dimensional (2D) physics such as charge-density waves and superconductivity.[1−5] The amount of intercalant that can be inserted into a host material is limited by the charge and size of the guest species and the ability of the host to maintain charge balance and structural stability.[4] The ionic nature of many guest species requires either a change of the host lattice oxidation states or the presence of atomic vacancies to maintain charge neutrality.[4] Most intercalation routes for metals involve ball milling or high-temperature processing of stoichiometric amounts of materials. Traditional approaches in chemical intercalation involve electrochemical intercalation. All of these intercalation routes generate and intercalate a charged species, thus limiting the intercalant concentration.[1−5]

Recently, we have developed a chemical, solution-based method whereby a reaction to generate a zerovalent copper species is performed in the presence of a layered material. We have shown that high densities, up to 60 atomic percent, of zerovalent copper metal can be intercalated into Bi_2Se_3 nanoribbons. The atom % of copper intercalant is controlled by either the concentration or the reaction time.[6] In this article, using a similar methodology, we demonstrate that this is general, whereby many other zerovalent metals can be intercalated into layered Bi_2Se_3 chalcogenide nanoribbons. We show that it is possible to intercalate many zerovalent guest species using a solution disproportionation redox reaction or carbonyl decomposition. These include: Ag, Au, Co, Cu, Fe, In, Ni, and Sn. Some interesting effects that could arise with intercalation are superconductivity, such as in Cu−Bi_2Se_3,[7−10] enhanced conductivity,[6] or possibly opening a surface state gap in topological insulator Bi_2Se_3. This method of zerovalent metal intercalation may also be extended to other layered materials.

2. EXPERIMENTAL SECTION

Bi_2Se_3 is a 2D-layered chalcogenide material (Figure 1A). It has a rhombohedral crystal structure (space group: D^5_{3d} ($R\bar{3}m$)) with shifted, hexagonal planes of bismuth and selenium. The bismuth and selenium layers stack along the c-axis repeating every five layers as Se(1)−Bi−Se(2)−Bi−Se(1). Each quintuple layer is bound by van der Waals forces at neighboring Se layers. Intercalant guest atoms can be accommodated in the van der Waals gap.[7−11]

As an initial example, to capture the chemical methodology presented in this article, Bi_2Se_3 nanoribbons intercalated with 5 (red) and 21 (blue) atomic percent cobalt using the procedure outlined below are shown in Figure 1, along with respective high-resolution transmission electron microscope (TEM) images and electron diffraction. The atomic percent of cobalt is determined by energy-dispersive X-ray (EDX) spectroscopy (Figure 1C) in a TEM on a single nanoribbon and confirmed on ensemble nanoribbons with X-ray photoelectron spectroscopy (XPS). The inset figures demonstrate that nanoribbon morphology is not altered with intercalation and no precipitates are observed on the surface of the ribbon (Figure 1B). The EDX shows that the ratio of Bi:Se remains unchanged although intercalation concentration of cobalt increases. The electron diffraction also shows a striking superlattice structure with high cobalt intercalant concentration that is consistent with the Bragg signature of a charge density wave, similar to that seen in other intercalant

Received: May 21, 2012
Published: July 25, 2012

 © 2012 American Chemical Society

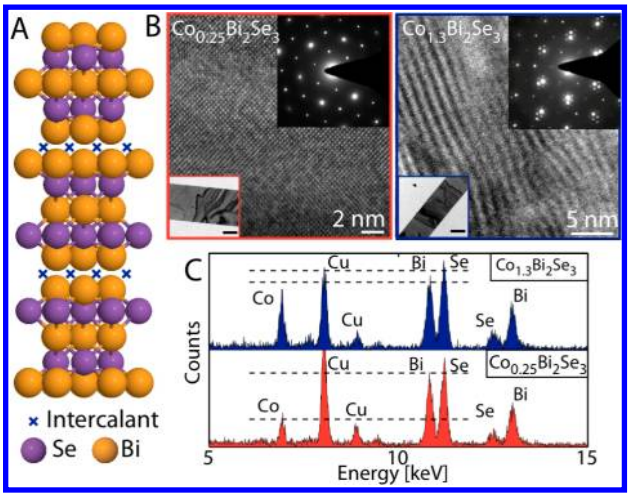

Figure 1. Bi_2Se_3 is a 2D layered host material with a van der Waals gap between successive layers that can accommodate intercalants (A). Transmission electron micrographs and electron diffraction patterns of nanoribbons of Bi_2Se_3, which can be intercalated with a variety of zerovalent metals, such as Co (B), to very high densities as determined by EDX (C), which do not alter the nanoribbon morphology (B; lower insets). With high densities of intercalant, superlattice patterns are observed (B; upper insets).

compounds.[12] The high-resolution image demonstrates the appearance of a stripe phase consistent with an incommensurate charge density wave.[13,14] A combination of EDX, TEM, electron diffraction, XPS, and XRD are used to verify intercalation of various zerovalent metal atoms into Bi_2Se_3 nanoribbons, as explained in detail in the later section.

We can intercalate several zerovalent metal atoms to very high concentrations (Table 1) into Bi_2Se_3 nanoribbons. All reactions are performed in low-boiling point solvents, such as acetone at 52 °C. For all reactions, we provide experimental details using a 10 mM solution on average. Higher intercalant concentrations can be achieved using longer reaction times or higher metal precursor concentrations.[6]

2.1. Nanoribbon Synthesis. Bi_2Se_3 nanoribbons are grown using the vapor−liquid−solid (VLS) method of Kong et al.[15] We use quartz substrates for growth because silicon substrates lead to electroless deposition of the metal atom on the growth substrate during intercalation. Nanoribbon yields are approximately 5 ± 3 mg. Nanoribbons are, on average, 50 nm thick with widths and lengths ranging from hundreds of nanometers to several micrometers. Nanoribbons grown by this method tend to have sharp edges and high crystallinity, which can enable maximum intercalation.

2.2. Intercalation: Disproportionation Redox Reactions. *2.2.1. Au, Cu, Ag, and Sn.* Intercalation reactions are given in Table 1. In a typical reaction, Bi_2Se_3 nanoribbons on the quartz growth substrate are added to a 10 mM solution of precursor(s) in acetone kept just under reflux (at 52 °C) for 10 min. The substrate is removed from solution and rinsed with hot ethanol and hot acetone (~45 °C). Prior to the reaction, glassware is cleaned in an acid or base bath and allowed to sit overnight in acidic distilled water to adjust the pH. The solution pH value varies from 4 to 6.5. The atom percent of intercalant is determined by EDX and XPS. The atom % of gold was determined using XPS; Au emission lines are overlapped by Bi and Se in EDX.

Silver disproportionates in the presence of a tetraazocyclic amine ligand.[20−24] Tin disproportionates in the presence of a tartrate or citrate.[25,26] These are added as precursors in excess to facilitate disproportion (Table 1).

2.2.2. In. Indium chloride disproportionates in dimethyl sulfoxide and in tetrahdyrofuran.[27−29] We have also found that InCl slowly disproportionates in acetone. Indium chloride is air sensitive; intercalation reactions are performed under inert N_2 atmosphere using standard Schlenck techniques. In a typical reaction, Bi_2Se_3 nanoribbons on a quartz growth substrate are placed into a round-bottom flask, which is evacuated and flushed with nitrogen. Air-free acetone (3 mL) from Sigma-Aldrich is added to the flask and heated to just below reflux (52 °C). Dropwise, a solution containing InCl (0.015 g from Sigma Aldrich) dissolved in 3 mL of acetone is added to the solution and kept just under reflux for up to one hour. The substrate is removed from solution and rinsed with hot ethanol and hot acetone (~45 °C).

2.2.3. Ni. Nickel(II) is reduced in the presence of hydrazine which decomposes and disproportionates.[30] Bi_2Se_3 on the quartz growth substrate is added to a vial of 10 mM nickel nitrate pentahydrate (Alfa Aesar) in acetone. Slowly, hydrazine hydrate (1 mL from Sigma Aldrich) is added to the solution. The reaction is allowed to sit for an additional 30 min. Nickel deposited on the substrate is removed by rinsing with hot ethanol and acetone.

2.3. Intercalation: Carbonyl Decomposition. *2.3.1. Fe and Co.* We intercalate cobalt and iron by the decomposition reaction of the associated carbonyls, dicobalt octacarbonyl and iron pentacarbonyl, in solution[31,32] under inert atmosphere. The substrate containing Bi_2Se_3 nanoribbons is placed in a round-bottom flask, evacuated and flushed with N_2 gas. Air-free acetone (5 mL from Sigma-Aldrich) is added to the flask and heated to reflux. Dicobalt octacarbonyl (0.03 g from Fisher Scientific) or iron pentacarbonyl (0.02 g from Sigma Aldrich) in 5 mL of acetone is dropwise added to the flask over the course of an hour. The solution is allowed to reflux for 1 h. Substrates were removed from the solution and rinsed with hot acetone and hot ethanol. At high concentrations, these reactions generate metal nanoparticles of iron and cobalt.[31] These particles are removed by rinsing with ethanol and acetone (25 °C) and/or via sonication of the nanoribbons. Iron pentacarbonyl should not decompose in acetone at 52 °C.[33] However, we were able to detect non-negligible amounts of iron in the Bi_2Se_3 nanoribbons, indicating the decomposition of trace

Table 1. Summary of the Elements Intercalated, Concentrations Attained, Reactions to Generate Zerovalent Species, and Precursor Chemistry[a]

intercalant	max atom, %	10 mM, 10 min, %	precursor(s)	reaction
copper	60	2.5	tetrakis(acetonitrile) copper(I) hexafluorophosphate	$2Cu^+_{(aq)} \rightarrow Cu^{2+}_{(aq)} + \mathbf{Cu(0)}$[16−18]
silver	>50	8.0	silver nitrate; 0.1 g 5,5,7,12,12,14-hexamethyl-1,4,8,11-tetraazocyclotetradecane	$2Ag^+ + L \rightarrow AgL^{2+} + \mathbf{Ag(0)}$[20−24]
tin	20	1.9	stannous chloride; 0.1 g tartaric acid	$2Sn^{2+} \rightarrow Sn^{4+} + \mathbf{Sn(0)}$[25,26]
gold	20	2	gold(I) chloride or chlorotristriphenylphosphine gold(I)	$3Au^+_{(aq)} \rightarrow Au^{3+}_{(aq)} + 2\mathbf{Au(0)}$[16,19]
indium	7	17	indium(I) chloride	$3InCl \leftrightarrow InCl_3 + 2\mathbf{In(0)}$[27−29]
cobalt	20	10.5	dicobalt octacarbonyl	$Co_2(CO)_8 \rightarrow 8CO + \mathbf{Co(0)}$
iron	7.5	3.0	iron pentacarbonyl	$Fe(CO)_5 \rightarrow 5CO + \mathbf{Fe(0)}$
nickel	2.1	0.8	nickel(II) nitrate pentahydrate; hydrazine hydrate	$2Ni^{2+} + N_2H_4 + 4OH^{-2} \rightarrow 2\mathbf{Ni(0)} + N_2 + 4H_2O$[33]

[a]L = tetraazocyclic amine ligand.

dx.doi.org/10.1021/ja304925t | J. Am. Chem. Soc. 2012, 134, 13773−13779

amount of iron pentacarbonyl. Iron and cobalt atom percentages are detected using TEM-EDX and XPS.

2.4. Control Experiments: Reactions That Do Not Produce Zerovalent Atoms in Solution. As a control, we performed several reactions in solution where no zerovalent atoms were produced, using salts with a valence of +2 or +3. This causes morphological and constitutional changes in the nanoribbon. Bismuth(III) ion is medium on the Pearson soft−hard acid−base scale;[34,35] most metal ions of these salts are softer acids. Acetone, a hard base, promotes exchange of the salt cation and bismuth in the nanoribbons.

2.4.1. Au^{2+}. Gold disproportionation favors acidic conditions; basic conditions result in a charged Au species. Reaction glassware is cleaned in a strong base bath (pH value 11), rinsed with water, and allowed to dry overnight. The solvent has a basic pH value of 8. We perform the intercalation reaction at this pH (8) with identical conditions using 10 mMol of gold(I) chloride in acetone. The nanoribbons show large voids.

2.4.2. Cu^{2+}. As a control, we used a divalent copper precursor salt, copper(II) nitrate from Alfa Aesar, rather than a monovalent salt. Nanoribbons on a substrate are added to a solution of 10 mM copper(II) nitrate from Alfa Aesar dissolved in 5 mL of acetone for 4 h at 25 °C. The sample is rinsed with acetone and ethanol upon removal. The resulting nanoribbon observed with TEM has voids. Performing the reaction at 52 °C results in complete exchange of bismuth with copper, forming copper selenide.

2.4.3. Ru^{3+}. Nanoribbons on a quartz substrate are added to a solution of $RuCl_3$ (0.025 g from Sigma-Aldrich) in 14 mL of acetone and 1 mL of 1,2-propanediol from Fisher Scientific and heated just below reflux for 4 h. Ruthenium exchanges for bismuth in the nanoribbons, forming polycrystalline domains and destroying the nanoribbon morphology.

2.5. Characterization. Several different characterization techniques are used to determine the elemental composition, structure, lattice constants, and oxidation states of the intercalant. In-situ transmission electron microscopy (TEM), diffraction, images, electron energy loss spectroscopy (EELS) spectra, and energy dispersive X-ray (EDX) were acquired on single nanoribbons on a FEI Tecnai G2 F20 at 200 kV with a Gatan double-tilt heating holder or on a FEI Titan 80-300 at 300 kV. X-ray diffraction (XRD) data were acquired using a PANalytical X'Pert using copper K-edge (1.54 Å) X-rays. Rietveld refinement is used to determine Bi_2Se_3 lattice constants post intercalation. X-ray photoelectron spectroscopy (XPS) data were collected with a PHI VersaProbe Scanning XPS Microprobe using Al(Kα) radiation (1486 eV). Ribbons were transferred to a silicon substrate for XPS measurement. Atomic structures were visualized using Jmol.[36]

2.6. Formation of Superlattices. With the exception of silver and copper, intercalants are not ordered after intercalation, or intercalant concentration was not high enough to induce ordering as measured in electron diffraction. Critical concentrations that allowed us to observe superlattice patterns were above 10 atomic percent. To induce intercalant ordering, the samples on the TEM grid are heated to 250 °C for 5 min under nitrogen or under vacuum. Nanoribbons were analyzed both before and after heating to observe superlattice formation.

3. RESULTS AND DISCUSSION

3.1. Evidence of Intercalation: Constant Bi:Se Ratio. With intercalation, the ratio of bismuth to selenium will not change as the atom percent of intercalant increases. If a chemical interaction occurs, such as an exchange reaction, this ratio is altered. We demonstrate for the variety of metal atom intercalants that as the intercalant concentration increases to superstoichiometric values, the Bi:Se ratio does not change (Figure 2). The elemental composition of single nanoribbons is detected using TEM-EDX. A stacked plot of the EDX spectra (Figure 2B), with all spectra normalized by the Bi 11 keV peak, shows that, regardless of intercalant, the Bi:Se ratio does not

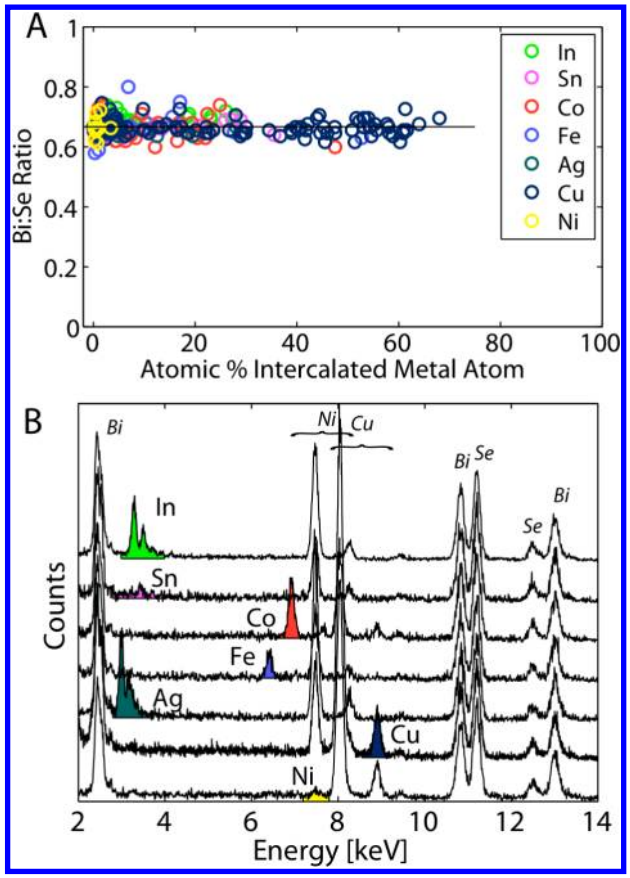

Figure 2. (A) EDX determinations of Bi:Se ratios show no dependence on guest species concentration. (B) Normalized stacked EDX spectra, showing elemental identification and constant Bi:Se ratios.

change. For these measurements, either Cu or Ni TEM grids are used, depending on the guest species, to minimize EDX peak overlap.

3.2. Intercalant Ordering into Superlattices. Single-crystal superlattice patterns, observed with electron diffraction, are a strong signature of intercalation.[1−4] Superlattice spots are additional reflections due to ordering of the intercalant in the host lattice.[2,37] Figure 3 demonstrates the wide variety of superlattice patterns observed in the highest intercalated concentrations (see Table 1) of Cu[6], Co, Ag, Sn, and Fe intercalated Bi_2Se_3. We expect that each metal atom species has specific preferred interstitial sites in the Bi_2Se_3 lattice and that, at high enough concentrations, the atoms interact to yield preferred long-range-ordered structures. These structures are very different even for atomic species that are very similar in size and/or typical chemical behavior; thus we are hesitant to suggest speculative explanations for the wide range of maximum loading and prefer to let the data speak for themselves. Nanoribbons were clearly free of nanoparticle precipitates in TEM images, and superposed diffraction patterns from the pure metallic elements (which would generally look like polycrystalline rings) are not observed. No superlattice pattern ever appears in the pure Bi_2Se_3 regardless of heat treatment, verifying that the superlattices are associated with the intercalants.

Both Co and Ag intercalated Bi_2Se_3 demonstrate strong satellite spots associated with each Bi_2Se_3 Bragg spot. Similar satellites have been widely recognized in superlattice intercalate

dx.doi.org/10.1021/ja304925t | J. Am. Chem. Soc. 2012, 134, 13773−13779

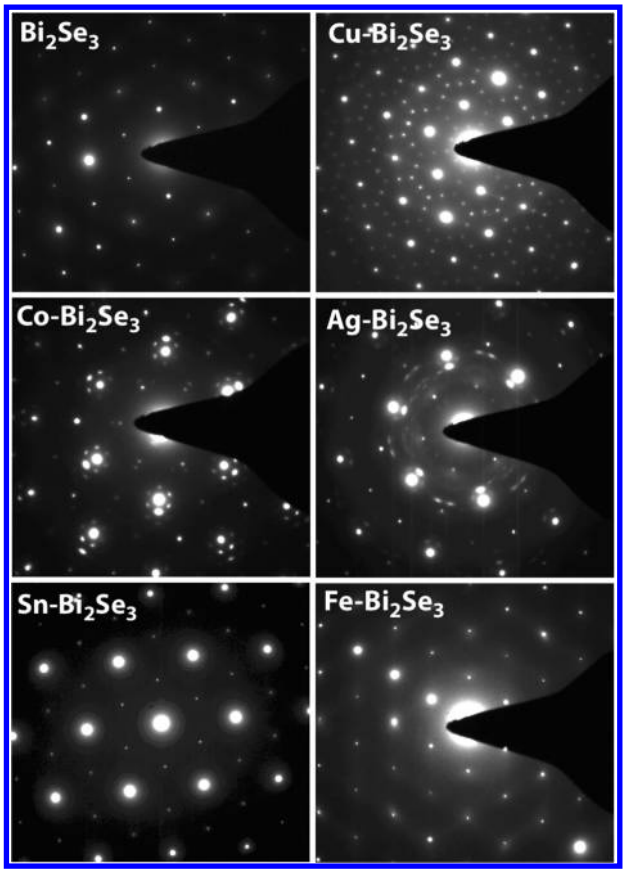

Figure 3. Superlattice patterns are observed with intercalation of zerovalent metal atoms, indicating interlayer ordering of atoms within Bi_2Se_3. Superlattice patterns can vary with concentration.

systems of a Bragg signature of an incommensurate charge density wave.[12] The satellite positions of Co−Bi_2Se_3 are consistent with a $(43a)^{1/2} \times (43a)^{1/2}$ superlattice, corresponding to a spacing of 1.36 nm with an 8° rotation. This spacing can be seen in a high-resolution TEM image (Figure 1) which reveals the stripe phase of the incommensurate charge density wave.[13,14]

Analysis of the diffraction pattern observed in intercalated Ag−Bi_2Se_3 is somewhat less precise and more open to interpretation due to the diffuse, azimuthally spread nature of the superlattice spots. The satellite positions are consistent with a 7 × 7 structure, suggestive of a slight (ratio of 7:6) mismatch in the natural periodicity of the Bi_2Se_3 host and the Ag intercalant layers. However, they may also be interpreted as a set of rotational variants of an incommensurate charge density wave with a periodicity of order 1.4 nm.

Intercalation of Fe, Au, and In forms a diffuse set of lines between nearby Bragg spots. This suggests disordering of the intercalant due to too low intercalant concentration to result in ordering or possibly the creation of crystal defects such as stacking faults in the host.

Intercalation of Sn and Ni forms a characteristic pattern of alternating bright and dark diffraction spots. The weak spots are forbidden in the fcc-like ABC stacking in the host Bi_2Se_3 lattice. Thus, the presence of these spots implies a breaking of the symmetry whereby the A, B, and C atomic columns no longer all have the same scattering amplitudes. A likely, but not unique, interpretation is that the intercalated atoms lie mostly in interstitial sites in the van der Waals gap and have sufficient ordering in the *c*-direction to break the symmetry. Figure 4B illustrates such a structure as viewed down the *c*-axis, along with

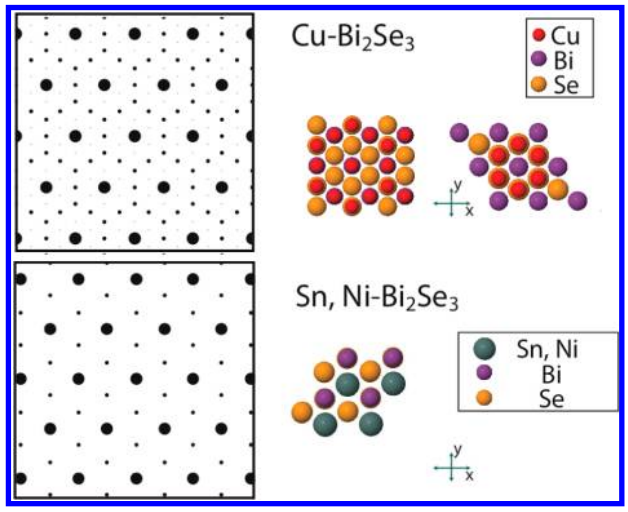

Figure 4. Simulated superlattice electron diffraction patterns and corresponding atomic structures of the ordered intercalant (Cu, Sn, and Ni) for electron diffraction patterns (Figure 3) that can be constrained.

a diffraction pattern calculated simply as the Fourier transform of the scattering density evaluated in the (001) plane.

Copper intercalation shows a far greater variety of intercalant ordering.[6] Most copper superlattice patterns are complex and difficult to analyze to determine the intercalant structural ordering. However, the highest intercalation densities (60%) in nanoribbons form a characteristic superlattice pattern (Figure 3) with a hexagon of 12 superlattice spots surrounding each of the host lattice spots (6 midway between adjacent bright spots—edge-centered spots, and 6 at the centers of equilateral triangles of bright spots—triangle-centered spots). The triangle-centered spots are the same forbidden spots seen in the Sn and Ni cases and can be associated with a periodic lattice distortion or interplanar stacking.[38,39] Edge-centered spots give information about the intercalant in-plane ordering. The superlattice spots are consistent with a structure based on hexagonal Cu_6 rings in a 2 × 2 × 1 superlattice (Figure 4; right structure), with disorder in the *c*-direction. Because of aspect ratios of the ribbons, high-quality diffraction patterns could not be obtained on zone axes other than [001]; thus, the solution for the structure is not unique. For example, the inverse structure (Figure 4; left structure, with Cu atoms swapped with Cu vacancies) is also consistent with the positions and intensities of the superlattice spots.

3.3. Evidence of Intercalation: Lattice Expansion. The strongest evidence of intercalation is observed in a change of the unit cell volume[1,3,40] and can be detected with X-ray diffraction. For all zerovalent intercalants in this study, the unit cell volume expands. Lattice constants were determined through Rietveld refinement of the XRD; elemental composition was determined through TEM-EDX and XPS. For comparison, samples with less than 10% intercalant are presented (Figure 5A). All demonstrate a noticeable increase in the unit cell volume. As the intercalant concentration is increased to substantial amounts, the unit cell volume increases sizably (Figure 5B). The different preferred bonding patterns of the individual elements (characterized for example by the pure-

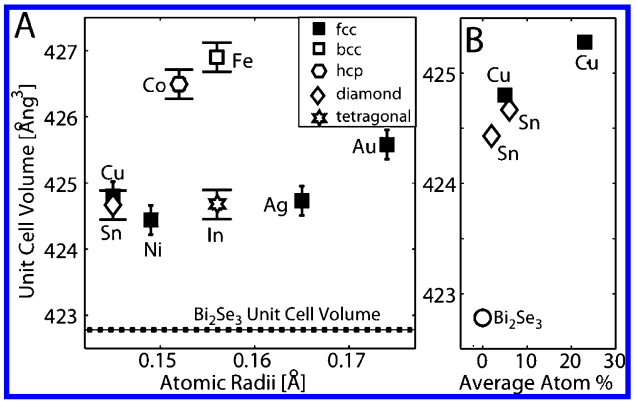

Figure 5. (A) X-ray diffraction shows expansion of the unit cell volume for average concentrations below 10 atomic percent. Favored bonding structure of the metal intercalant may also influence the lattice expansion. (B) The host unit cell volume also expands with increasing atom %.

element crystal structure) are shown in Figure 5, indicating that there is no direct correlation.

3.4. Evidence of Intercalation: Control Experiments. In Figure 2 we showed that, during intercalation, the ratio of Bi:Se does not change. We further established that the intercalants are zerovalent by performing control experiments using other salts and reactions that, in solution, will produce 2+ or 3+ valent ions and no zerovalent species. These reactions favor cation exchange over intercalation.[41−43]

In Figure 6B, examples with Au^{2+}, Cu^{2+}, and Ru^{3+} salts are shown, demonstrating that the Bi:Se ratio is altered. The nanoribbon morphology and overall structure (Figure 6A) are also altered in stark contrast to intercalation. Both Cu^{2+} and Au^{2+} produce voids in the nanoribbon due to volume change of the crystal. For ruthenium, an ion-exchange reaction occurs,

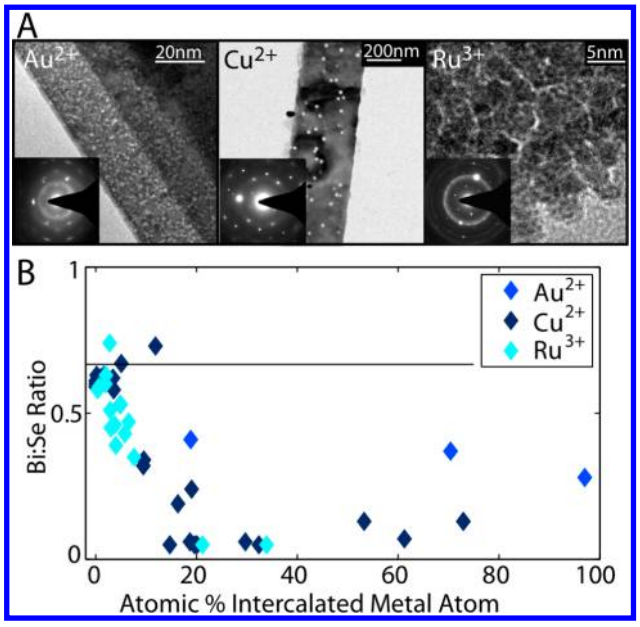

Figure 6. As a control experiment, reactions that do not yield zerovalent metal atoms in solution, only multivalent species, result in exchange of bismuth with the cation leading to large voids in the nanoribbon, in the case of Cu^{2+} and Au^{2+}, or destruction of the single-crystal morphology, as with Ru^{3+}. Diffuse rings are observed in electron diffraction.

forming polycrystals from the nanoribbon. EDX spectra identify the composition of these nanoribbons as follows: Figure 6 left: 5% Au, 40% Bi, 55% Se. Figure 6 middle: 4% Cu, 33% Bi, 63% Se. Figure 6 right: 4% Ru, 33% Bi, 63% Se. For all examples shown, diffuse polycrystalline rings are observed in the electron diffraction unlike intercalated samples. These examples can be compared to Figure 1, clearly demonstrating that, in an intercalation reaction, the nanoribbon morphology and structure are not destroyed with intercalation.

3.5. Zerovalent Identification of Intercalants. The strongest evidence for the zerovalent nature of the metal atom intercalants lies in our ability to intercalate super-stoichiometric amounts with changing the oxidation states of the host materials. The atom % of intercalant would otherwise be limited by the charge of the guest species.[4] It is possible in some intercalation reactions to further identify the oxidation state using spectroscopic signatures.

We previously identified the oxidation state of copper intercalated in Cu−Bi_2Se_3 as Cu(0) using XPS and EELS.[6] EELS is a powerful technique to identify the oxidation states of a transition metal based on the near-edge fine structure, such as the L_3/L_2 ratio.[44,45] Of the intercalants here, Co, Fe, and Ni have accessible EELS edges. We use the method of reference[45−48] to determine the L_3/L_2 ratio of Co from the EELS spectra (Figure 7A) with 30 atom % Co. The L_3/L_2 ratio is 3.65 ± 0.2, the white line intensity region of Co(0).[49] The shape of the EELS spectra and the white line intensity ratio are

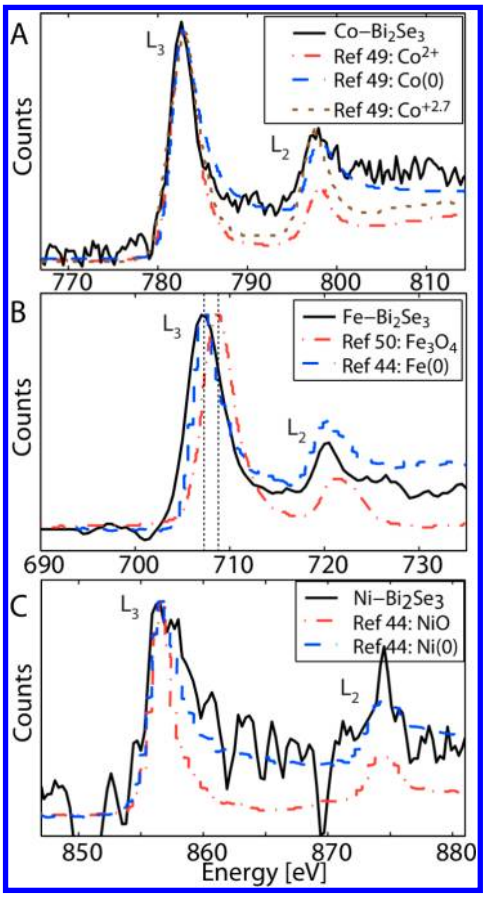

Figure 7. EELS spectra of Co, Fe, Ni intercalated Bi_2Se_3 nanoribbons plotted with reference spectra,[44,49,50] confirm that intercalated metals are zerovalent by the ratio of the L_3 to L_2 edges and spectral shape and position.

dx.doi.org/10.1021/ja304925t | J. Am. Chem. Soc. 2012, 134, 13773−13779

identical to those observed in ref 49 for Co(0). Thus, intercalated cobalt is zerovalent, Co(0).

Similarly, we show that Fe and Ni are zerovalent. The shape and the position of the L_3 and L_2 peaks in the EELS spectra of 7.5 atom % Fe and 1.2 atom % Ni intercalated Bi_2Se_3 nanoribbons match Fe(0) and Ni(0) reference spectra.[44] Examples are shown of Fe_3O_4 and NiO for comparison.[44,50] The fluctuation of the spectra in Figure 7C is due to the relatively low concentration (1.2 atom %) of Ni intercalant. All the experiments performed for this work point to no detectable charge transfers between intercalants and Bi_2Se_3. However, very small charge transfer, nondetectable by EELS, could still occur.

3.6. Discussion of Intercalation and Ion Exchange. In traditional approaches, intercalation of large concentrations of charged guest species tends to cause large structural changes or to induce significant charge transfer between the guest and the host. Zerovalent intercalation reactions demonstrated here are peculiar because they impose low charge transfer and structural constraints on the host. In the sole previous example in the literature of the superstoichiometric, zerovalent intercalation of Hg into TiS_2, it is hypothesized that the driving force of intercalation is the energy stabilization of the intercalated mercury network compared to that of liquid mercury.[51] It is known that metals have nearly zero solubility in common organic solvents. In our case, zerovalent metal atoms generated in organic solvent have little solvation energy that would stabilize them in solution so that there is a strong thermodynamic driving force for them to enter the solid state either by intercalating into a host or by crystallizing and forming precipitates. In our experimental conditions, very low concentrations of zerovalent metal atoms are generated, making homogeneous nucleation of crystalline precipitates unlikely. Interestingly, heterogeneous nucleation of precipitates is also suppressed in almost all cases so that these zerovalent metal atoms are preferentially stabilized by intercalation into the 2D host. This may in part be due to kinetics, since a single metal atom may diffuse directly into the host while the nucleation of a precipitate requires the simultaneous assembly of rather a large number of metal atoms, which is unlikely at low metal atom concentrations. However, we also observe that the intercalated materials are stable for months after the reactions, suggesting that either the intercalated state is more stable than the pure metal precipitate, or the free energy difference is small enough that a critical nucleus is unlikely to form. Quantum chemistry calculations together with long-term observations will be needed to form a definitive answer to this question, which may vary with intercalant species.

We also observe that, under conditions favorable for metal atom intercalation, cation exchange either did not occur or proceeded at immeasurably slow rates. This indicates a difference in kinetics since, for example in the case of Cu, the concentrations of Cu(0) and Cu(II) in solution were roughly equal after disproportionation. The introduction of a single metal atom into a host must only overcome the activation energy associated with atomic diffusion, while the exchange of one cation for another involves the breaking of bonds and, one supposes, a higher activation energy. Again, this is a question requiring computation and additional experiments for a definitive answer, and the answer may be different for different intercalants.

4. CONCLUSION

We have provided a general chemical method for intercalating zerovalent metal atoms into Bi_2Se_3 nanoribbons and provide solid evidence for zerovalent metal atom intercalation. (i) XRD shows lattice expansion with intercalation. (ii) Superlattice patterns associated with intercalation appear for many atomic intercalants. (iii) There is no indication of precipitates; i.e. no rings are observed in electron diffraction nor is there any indication of precipitates. (iv) Nanoribbon morphology is also unaffected. (v) The ratio of Bi:Se with intercalation is unchanged. Additional EELS spectral signatures, where possible, verify intercalated atoms possess a zerovalent oxidation state.

This investigation offers a new method to readily intercalate zerovalent metal atoms into Bi_2Se_3 nanoribbons without disrupting the host lattice. We foresee the potential impact of this methodology in establishing fundamentally new and unexpected physical behaviors as well as a new method of atomic storage for possible energy or catalytic materials applications. This methodology appears to be general and may be used to intercalate zerovalent metals into other 2D layered nanomaterials.

■ ASSOCIATED CONTENT

Ⓢ Supporting Information

Additional high-resolution TEM images, XPS data, and XRD data. This material is available free of charge via the Internet at http://pubs.acs.org.

■ AUTHOR INFORMATION

Corresponding Author

yicui@stanford.edu

Notes

The authors declare no competing financial interest.

■ ACKNOWLEDGMENTS

We thank T. Geballe for his invaluable insight in this work. Y.C. acknowledges support from the Department of Energy, Office of Basic Energy Sciences, Materials Sciences and Engineering Division, under contract DE-AC02-76-SFO0515. B.W.R. was supported through grants by the U.S. Department of Energy, Office of Basic Energy Sciences, Division of Materials Science and Engineering, and work was performed under the auspices of the U.S. Department of Energy by LLNL under Contract No. DE-AC52-07NA27344.

■ REFERENCES

(1) Müller-Warmuth, W., Schöllhorn, R., Eds. *Progress in Intercalation Research*; Kluwer: Dordrecht, The Netherlands, 1994.

(2) Dresselhaus, M. S., Ed. *Intercalation in Layered Materials*; NATO ASI Series, Subseries B, Physics; Plenum Press: New York, 1987; Vol. *148*.

(3) Levy, F., Ed. *Intercalated Layered Materials*; Reidel: Dordrecht, The Netherlands, 1979.

(4) Whittingham, M. S., Jacobson, A. J., Eds. *Intercalation Chemistry*; Academic Press: New York, 1982.

(5) Whittingham, M. S. *J. Solid State Chem.* **1979**, *29*, 303−310.

(6) Koski, K. J.; Cha, J. J.; Reed, B. W.; Wessels, C.; Kong, D.; Cui, Y. *J. Am. Chem. Soc.* **2012**, *134*, 7584−7587.

(7) Hor, Y. S.; Williams, A. J.; Checkelsky, J. G.; Roushan, P.; Seo, J.; Xu, Q.; Zandbergen, H. W.; Yazdani, A.; Ong, N. P.; Cava, R. J. *Phys. Rev. Lett.* **2010**, *104*, 057001/1−057001/4.

(8) Hor, Y. S.; Checkelsky, J. G.; Qu, D.; Ong, N. P.; Cava, R. J. *J. Phys. Chem. Solids* **2011**, *72*, 572−576.
(9) Wray, L. A.; Xu, S.-Y; Xia, Y.; Hor, Y. S.; Qian, D.; Fedorov, A. V.; Lin, H.; Bansil, A.; Cava, R. J.; Hasan, M. Z. *Nat. Phys.* **2010**, *6*, 855−859.
(10) Kriener, M.; Segawa, K.; Ren, Z.; Sasaki, S.; Ando, Y. *Phys. Rev. Lett.* **2011**, *106*, 127004/1−127004/4.
(11) Vaško, A.; Tichý, L.; Horák; Weissenstein. *J. Appl. Phys.* **1974**, *5*, 217−221.
(12) Wilson, J. A.; Di Salvo, F. J.; Mahajan, S. *Adv. Phys.* **1975**, *24*, 117−201.
(13) Chen, C. H.; Gibson, J. M.; Fleming, R. M. *Phys. Rev. B* **1982**, *26*, 184−205.
(14) Clarke, R.; Elzinga, M.; Gray, J. N.; Homma, H.; Morelli, D. T.; Winokur, M. J.; Uher, C. *Phys. Rev. B* **1982**, *26*, 5250−5253.
(15) Kong, D.; Dang, W.; Cha, J. J.; Li, H.; Meister, S.; Peng, H.; Liu, Z.; Cui, Y. *Nano Lett.* **2010**, *10*, 2245−2250.
(16) MacKay, K. M. *Introduction to Modern Inorganic Chemistry*, 6th ed.; CRC Press: Boca Raton, FL, 2002.
(17) Sidgwick, N. V. *The Chemical Elements and Their Compounds*; Clarendon Press: Oxford, 1950; Vol. *1*, pp 106−108.
(18) Wu, J.; Liu, D.; Zhou, J.-G.; Hagelberg, F. *J. Phys. Chem. A* **2007**, *111*, 4748−4758.
(19) Gammons, C. H.; Yu, Y.; Williams-Jones, A. E. *Geochim. Cosmochim. Acta* **1997**, *61*, 1971−1983.
(20) Kester, M. O.; Allred, A. L. *J. Am. Chem. Soc.* **1972**, *94*, 7189−7189.
(21) Grzejdziak, A. *Monatsh. Chem.* **1994**, *125*, 107−117.
(22) Barefield, E. K.; Mocella, M. *Inorg. Chem.* **1973**, *12*, 2829−2832.
(23) Olejniczak, B.; Dziegie'c, J.; Grzejdziak, A. *Monatsh. Chem.* **1997**, *128*, 13−21.
(24) Swisher, R. G.; Stuehr, D. J.; Knox, J.; Fox, B. M.; Blinn, E. L. *J. Coord. Chem.* **1989**, *20*, 101−107.
(25) Gadolin, J. K. *Sv. Vet. Acad. Handl.* **1788**, 186−197.
(26) Gadolin, J. *Crells Chem. Annal.* **1790**, *1*, 260−273.
(27) Schneider, U.; Kobayashi, S. *Angew. Chem.* **2007**, *119*, 6013−6016.
(28) Pikunov, A. V.; Maslennikov, S. V.; Spirina, I. V.; Artemov, A. N.; Maslennikov, V. P.; Russ.. *J. Gen. Chem.* **2002**, *72*, 1323−1326.
(29) Piercy, R.; Hampson, N. A. *J. Appl. Electrochem.* **1975**, *5*, 1−15.
(30) Li, Z.; Han, C.; Shen, J. *J. Mater. Sci.* **2006**, *41*, 3473−3480.
(31) Thomas, J. R. *J. Appl. Phys.* **1966**, *37*, 2914−2915.
(32) van Wonterghem, J.; Morup, S.; Charles, S. W.; Wells, S.; Villadsen, J. *Phys. Rev. Lett.* **1985**, *55*, 410−413.
(33) Dewar, J.; Jones, H. O. *Proc. R. Soc. Lond. A* **1907**, *79*, 66−80.
(34) Pearson, R. G. *J. Am. Chem. Soc.* **1963**, *85*, 3533−3539.
(35) Ho, T.-L. *Chem. Rev.* **1975**, *75*, 1−20.
(36) Jmol: an open-source Java viewer for chemical structures in 3D. http://www.jmol.org/
(37) Parry, G. S.; Scruby, C. B.; Williams, P. M. *Philos. Mag.* **1974**, *29*, 601−612.
(38) Tatlock, G. J.; Acrivos, J. V. *Philos. Mag. B* **1978**, *38*, 81−93.
(39) Beal, A. R.; Liang, W. Y. *Philos. Mag.* **1973**, *27*, 1397−1416.
(40) Powell, A. V. *Annu. Rep. Prog. Chem., Sect. C: Phys. Chem.* **1993**, *90*, 177−213.
(41) Dloczik, L.; Könenkamp, R. *Nano Lett.* **2003**, *3*, 651−653.
(42) Son, D. H.; Hughes, S. M.; Yin, Y.; Alivisatos, A. P. *Science* **2004**, *306*, 1009−1012.
(43) Robinson, R.; Sadtler, B.; Demchenko, D. O.; Erdonmez, C. K.; Wang, L.-W.; Alivisatos, A. P. *Science* **2007**, *317*, 355−358.
(44) Leapman, R. D.; Grunes, L. A.; Fejes, P. L. *Phys. Rev. B* **1982**, *26*, 614−635.
(45) Egerton, R. F. *Rep. Prog. Phys.* **2009**, *72*, 016502/1−016502/25.
(46) Wang, Z. L.; Yin, J. S.; Jiang, Y. D. *Micron* **2000**, *31*, 571−580.
(47) Pearson, D. H.; Ahn, C. C.; Fultz, B. *Phys. Rev B* **1993**, *47*, 8471−8478.
(48) Pearson, D. H.; Fultz, B.; Ahn, C. C *Appl. Phys. Lett.* **1988**, *53*, 1405−1407.
(49) Vodungbo, B.; Zheng, Y.; Marangolo, M.; Demaille, D.; Varalda, J. *J. Phys.: Condens. Matter* **2007**, *19*, 116205/1−116205/8.
(50) Quintana, C.; Menéndez, J. L.; Huttel, Y.; Lancin, M.; Navarro, E.; Cebollada, A. *Thin Solid Films* **2003**, *434*, 228−238.
(51) Lemaux, S.; Golub, A. S.; Gressier, P.; Ouvrard, G. *J. Solid State Chem.* **1999**, *147*, 336−340.